Chinese Chemical Letters 35 (2024) 108467

Contents lists available at ScienceDirect

Chinese Chemical Letters

journal homepage: www.elsevier.com/locate/cclet

# Cisplatin-appended BODIPY for near infrared II fluorescent and photoacoustic imaging-guided synergistic phototherapy and chemotherapy of cancer

Xuejian Xing, E Pang, Shaojing Zhao, Tangna Pan, Qiuxia Tan, Benhua Wang, Xiangzhi Song, Minhuan Lan*

*Key Laboratory of Hunan Province for Water Environment and Agriculture Product Safety, College of Chemistry and Chemical Engineering, Central South University, Changsha 410083, China*

ARTICLE INFO

*Article history:*
Received 2 February 2023
Revised 13 April 2023
Accepted 17 April 2023
Available online 18 April 2023

*Keywords:*
Phototherapy
Chemotherapy
Cisplatin
Bodipy
NIR II fluorescent imaging

ABSTRACT

Combining phototherapy and chemotherapy has been considered a promising modality for cancer therapy due to their synergistic effect. Herein, we developed three D-$\pi$-A-structured boron dipyrromethenes (BODIPYs) (named as **B-B**, **B-C**, and **B-C-Pt**). Due to their enlarged $\pi$-conjugated structure and high intramolecular charge transfer effect, the synthesized BODIPYs had photothermal conversion capability, and their absorption and fluorescence spectra were red-shifted. The cisplatin-appended BODIPY (**B-C-Pt**) exhibited good singlet oxygen ($^1O_2$) generation ability and near infrared (NIR) absorption and fluorescence ($\lambda_{Abs}$ = 748 nm, $\lambda_{Em}$ = 947 nm). After being encapsulated by distearoyl phosphoethanolamine polyethyleneglycol 2000 (DSPE-PEG-2000), which could inhibit the H-aggregation of **B-C-Pt**, the absorption and fluorescence of the obtained **B-C-Pt** nanoparticles (NPs) were red-shifted to 762 and 985 nm, respectively. The $^1O_2$ quantum yield and photothermal conversion efficiency of the **B-C-Pt** NPs were 4.0% and 40.6%, respectively. Moreover, **B-C-Pt** NPs had chemotherapeutic efficacy due to the presence of cisplatin. *In vitro* and *in vivo* studies further demonstrated that **B-C-Pt** NPs had synergistic therapeutic efficacy. Together, **B-C-Pt** NPs could be employed in NIR II fluorescent and photoacoustic imaging-guided synergistic phototherapy and chemotherapy for cancer treatment.



The phototherapeutics in the ground state ($S_0$) transits to a singlet excited state ($S_1$) after absorbing photo energy, but it is unstable, can release heat by vibrational relaxation for photothermal therapy (PTT). In addition, $S_1$ converts into excited triplet state ($T_1$) by intersystem cross, which reacts with oxygen and water by electron transfer or energy transfer to generate reactive oxygen species (ROS) for photodynamic therapy (PDT) [1,2]. However, insufficient oxygen in tumor tissue and heat shock proteins (HSPs) expressed by heat stimuli can compromise the therapeutic efficacy of PDT and PTT, respectively [3,4]. Combining PDT with PTT can effectively enhance the therapeutic efficacy because heat generated by PTT can enlarge the blood vessels and enhance oxygen concentration in tumor tissue, while ROS generated by PDT can destroy the molecular structure and biofunction of HSPs, which is beneficial to the effectiveness of PTT [5–7].

In contrast to phototherapy, which is only effective in the area irradiated by light, chemotherapy uses drugs with cytotoxicity for treating cancer, is a systemic and effective method, especially for metastatic tumor because the drug could be delivered to cancer cells through blood circulation [8,9]. Chemotherapeutic drug can damage DNA, interfere the synthesis of DNA and RNA, inhibit the expressions of tumor-related proteins and cytokines, and active immune system to kill tumor cells or inhibit their growth. But long-term administration of chemotherapeutic drugs can lead to drug resistance, which can then lower the efficacy of the therapy [10–12]. Thus, developing multifunctional platform that can synchronously provide the effects of chemotherapy and phototherapy could significantly improve the therapeutic efficacy [13–15]. Besides its benefits mentioned above, combination therapy has many other advantages as follows: (i) ROS generated by PDT may destroy the cell membrane, thus improving its permeability, which can further increase the drug uptake; (ii) mitochondrial dysfunction caused by ROS can downregulate the expression of P-glycoprotein and thus suppress intracellular drug efflux; (iii) heat generated by PTT could further promote delivery and penetration of drug into deeper tumor tissue; and (iv) chemotherapy has a long-term effect, *e.g.* it could prevent tumor recurrence and metastasis [16–20].

* Corresponding author.
*E-mail address:* minhuanlan@csu.edu.cn (M. Lan).

https://doi.org/10.1016/j.cclet.2023.108467
1001-8417/

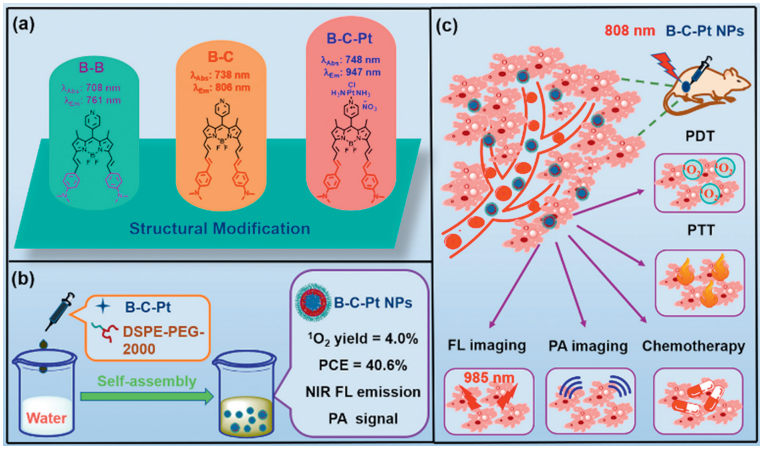


**Fig. 1.** (a) Molecular structures and absorption and fluorescence wavelengths of **B-B**, **B-C**, and **B-C-Pt**. (b) Preparation and main properties of **B-C-Pt** NPs. (c) Illustration of **B-C-Pt** NPs for fluorescent and PA imaging-guided synergistic PDT, PTT, and chemotherapy.

Generally, phototherapeutic and chemotherapeutic agents are co-loaded into nanomaterials, such as $SiO_2$, metal organic framework, and black phosphorus nanosheet through $\pi$-$\pi$ stacking or electrostatic interactions [21–24]. They can also be co-encapsulated in amphiphilic polymer to form water-dispersive nanoparticles (NPs) that could be used as a multifunctional platform for synergistic phototherapy and chemotherapy [25,26]. However, these hybrid nanodrugs have complex preparation processes and low stability, and uncontrollable release [27,28]. Integrating phototherapeutic and chemotherapeutic agents into a single molecule may be a promising approach to solve the above problems [29,30].

Boron dipyrromethene (BODIPY) is an excellent phototherapeutics because of its high extinction coefficient, excellent photostability, and easily modifiable structure [31–33]. BODIPY has been chelated with heavy metal atoms, such as Pt, Ir, and Ag, to enhance its spin-orbit coupling and further improve its singlet oxygen ($^1O_2$) generation capability [34–36]. Among these modified BODIPYs, Pt-appended BODIPY has been demonstrated to probably be suitable for combination therapy based on chemotherapy and phototherapy [37,38]. Huang *et al.* have synthesized visible light-excited platinum-BODIPY for synergistic PDT and chemotherapy [39]. However, the efficacy of PDT using these drugs in deep-seated lesions is compromised by the low penetrability of visible light. Chakravarty *et al.* have developed platinum-BODIPY conjugates with near infrared (NIR) emission and $^1O_2$ generation capacity under 715 nm laser irradiation. The BODIPY also has chemotherapeutic efficacy, but its photothermal performance was not evaluated [40]. Chen *et al.* have synthesized cisplatin-bearing BODIPY (BODIPY-Pt) and used it in phototherapy. Under 660 nm light irradiation, the BODIPY-Pt has $^1O_2$ quantum yield and photothermal conversion efficiency (PCE) of 31% and 28%, respectively [41]. However, its chemotherapy efficacy is not obvious. Development of NIR laser-excited BODIPY-platinum complex with phototherapeutic and chemotherapeutic efficacy can be of clinical significance.

Herein, we developed three d-$\pi$-A-structured BODIPYs (Fig. 1a), namely **B-B**, **B-C**, and the cisplatin-appended BODIPY (**B-C-Pt**), with high molar extinction coefficients ($\sim$1.0 $\times$ $10^5$ L $mol^{-1}$ $cm^{-1}$), sequentially red-shifted optical spectra, and increased photothermal conversion capability. Owing to the largest conjugated structure and the strongest intramolecular charge transfer (ICT) effect originated from pyridyl platinum, **B-C-Pt** exhibited NIR absorption and fluorescence peaks at 748 and 947 nm, respectively. Moreover, owing to the heavy atom effect caused by Pt, **B-C-Pt** had better $^1O_2$ production ability. **B-C-Pt** was further encapsulated by distearoyl phosphoethanolamine polyethyleneglycol 2000 (DSPE-PEG-2000) to prepare water-dispersive **B-C-Pt** NPs (Fig. 1b). These NPs exhibited red-shifted NIR absorption and fluorescence peaks at 762 and 985 nm, respectively. The **B-C-Pt** NPs had $^1O_2$ quantum yield and PCE of 4.0% and 40.6%, respectively, which show that they are suitable for PDT and PTT of cancer. The presence of cisplatin makes **B-C-Pt** cytotoxic to tumor and thus can be applied in chemotherapy. *In vitro* and *in vivo* studies revealed that **B-C-Pt** NPs could be employed in NIR fluorescent and photoacoustic (PA) dual-model imaging-guided synergistic phototherapy and chemotherapy for cancer therapy (Fig. 1c). This work presents an excellent example on the design of effective multifunctional nanoplatform for synergistic phototherapy and chemotherapy.

Three D-$\pi$-A-structured BODIPYs, named **B-B**, **B-C**, and **B-C-Pt**, were designed and synthesized (Fig. 1a). The molecular design strategy presented in this work has the following advantages. (i) 1,3,5,7-Tetramethyl-BODIPY has high extinction coefficient and highly electron-deficient property, thus was used as fluorophore and electron-withdrawing group. (ii) The incorporation of strong electron-donating group, *N,N*-dimethylaniline, into BODIPY can provide ICT effect, which resulted in the red-shift of the absorption and emission spectra to NIR region. (iii) The C=C bonds formed between *N,N*-dimethylaniline and BODIPY could further enlarge the conjugated structure; and the more the number of C=C bond, the larger the conjugated structure, and the longer the absorption and emission wavelengths. Moreover, the presence of two C=C bonds could significantly increase the photothermal conversion ability of **B-C** due to the high vibration of C=C. (iv) The symmetrical molecular structure and the introduction of electron-withdrawing group pyridine-platinum salt can greatly enhance the ICT effect of BODIPY. (v) The introduction of cisplatin provides it with chemotherapeutic efficacy; thus, it can potentially be used in synergistic chemotherapy and phototherapy. The detailed synthesis and characterization of BODIPYs are presented in Scheme S1 and Figs. S1–S8 (Supporting information).

The absorption and fluorescence spectra of BODIPYs in tetrahydrofuran (THF) presented in Fig. 2a showed that the absorption peaks of **B-B**, **B-C**, **B-C-Pt** were red-shifted from 707 and 738 nm to 748 nm; their extinction coefficient was also high with a value of $\sim$1.0 $\times$ $10^5$ L $mol^{-1}$ $cm^{-1}$ (Table S1 in Supporting information). The corresponding fluorescence peaks were also red-shifted from 761 and 806 nm to 947 nm (Fig. 2b). The red-shift observed in the spectra of **B-B** and **B-C** is due to their enlarged $\pi$-structure, while the significant red-shift observed in **B-C-Pt** is due to the strong ICT effect originated from pyridine-platinum salt [42,43]. Using zinc phthalocyanine (Zn-Pc) as a reference, the fluorescence quantum yield (FLQY) of **B-B**, **B-C**, and **B-C-Pt** were measured to be 21.5%, 2.6%, and 0.1%, respectively (Table S1 and Fig. S9 in Supporting in-

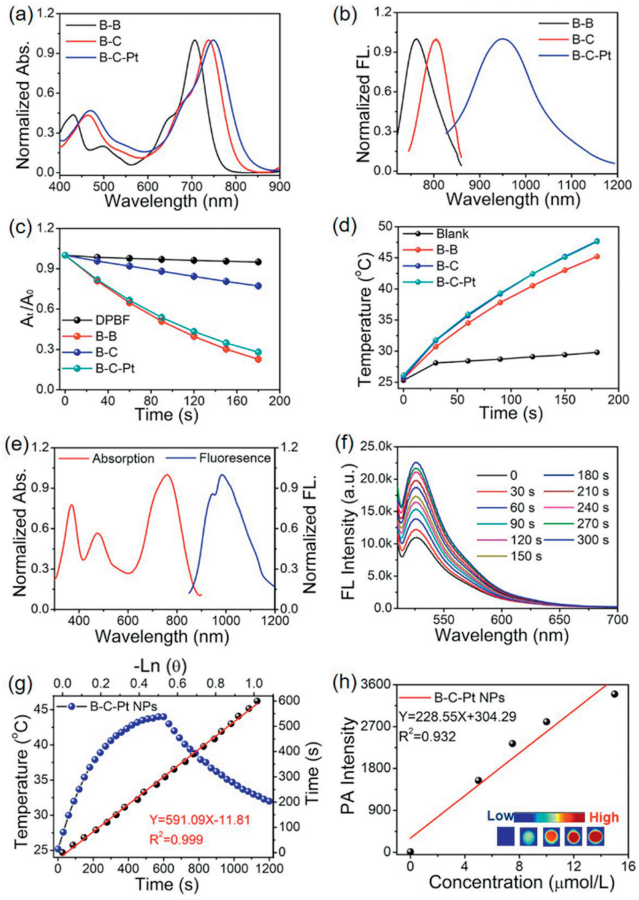


**Fig. 2.** (a) Normalized visible-near infrared (vis-NIR) absorption and (b) fluorescence spectra of **B-B**, **B-C**, and **B-C-Pt** in THF. (c) Change of absorbance ratio at 413 nm of DPBF with irradiation time in the presence of **B-B**, **B-C**, and **B-C-Pt**. (d) Variation of temperature with irradiation time of **B-B**, **B-C**, and **B-C-Pt** in DMSO solution. (e) Normalized vis-NIR absorption and fluorescence spectra of **B-C-Pt** NPs aqueous solution. (f) Change of fluorescence spectra of SOSG induced by **B-C-Pt** NPs under 808 nm laser irradiation (0.5 W/cm$^2$). (g) Variation of temperature of **B-C-Pt** NPs solution during irradiation with 808 nm laser for 10 min and non-irradiation for 10 min (blue curve), and linear plot of $-\ln(\theta)$ *versus* time (red curve). (h) PA intensity and images of **B-C-Pt** NPs solution at different concentrations (For interpretation of the references to color in this figure legend, the reader is referred to the web version of this article).

formation). The gradual decrease of FLQY may be ascribed to the higher number of rotatable C=C bonds in **B-C** and the heavy atom effect of Pt in **B-C-Pt** [44,41].

The $^1O_2$ generation of BODIPYs in THF was investigated using 1,3-diphenylisobenzofuran (DPBF) as a $^1O_2$ trapper [45]. The absorbance at 413 nm of DPBF decreased with increasing laser irradiation time (Fig. 2c and Fig. S10 in Supporting information). **B-C** had weaker $^1O_2$ generation capability than **B-B** because of the more non-radiative transition of **B-C** from the excited state to the ground state. In contrast, the $^1O_2$ generation capability of **B-C-Pt** was significantly increased due to the heavy atom effect. The photothermal conversion ability of BODIPYs in dimethyl sulfoxide (DMSO) was studied through temperature change upon being irradiated with 735 nm laser (Fig. 2d). After 3 min of laser irradiation, the temperature of **B-B**, **B-C**, and **B-C-Pt** solutions increased to 45.2, 47.7, and 47.6 °C, respectively. This suggests that the more rotatable C=C bonds in **B-C** and **B-C-Pt**, the better photothermal conversion capability. Further, the photothermal cycle and photostability of **B-C-Pt** were measured (Fig. S11 in Supporting information), reflecting the limited photothermal stability of **B-C-Pt**, which attributes to its poor photostability, but is beneficial for *in vivo* elimination. Based on its excellent photophysical and photochemical properties in organic solvents, including NIR absorption and fluorescence, excellent $^1O_2$ generation ability, and high photothermal conversion capability, **B-C-Pt** maybe a good candidate for phototherapy of cancer.

The aggregate type of **B-C-Pt** was studied in $H_2O$/DMSO mixture (Fig. S12 in Supporting information). The absorption and fluorescence peaks of **B-C-Pt** in DMSO appeared at 772 and 985 nm, respectively. As the ratio of $H_2O$ in the mixture was increased, the absorbance and fluorescence intensity of **B-C-Pt** gradually decreased, and the absorption was blue-shifted to 718 nm. This indicates that the aggregation of **B-C-Pt** in water is the H-type aggregation [46,47].

**B-C-Pt** was encapsulated by DSPE-PEG-2000 to generate water-dispersive NPs. We hypothesized that the long alkyl chain of DSPE-PEG-2000 not only provides a lipophilic microenvironment in the core of NPs, but also may insert into the space between two **B-C-Pt** molecules to inhibit their H-type aggregation. As a result, the absorption of **B-C-Pt** NPs was red-shifted to 762 nm (Fig. 2e). The first fluorescence peaked at 947 nm may belong to the fluorescence of **B-C-Pt** on the surface of NPs. The second fluorescence peaked at 985 nm ascribes to the fluorescence of aggregated **B-C-Pt** in the NPs, which is in the NIR II region, an indication that they may be suitable for NIR II fluorescence imaging. The scanning electron microscope (SEM) image revealed that the NPs had spherical morphology (Fig. S13a in Supporting information). The size distribution of these NPs is from 38 nm to 396 nm (Fig. S13b in Supporting information). The mean size of NPs is ~130 nm and has no obvious change after one week (Fig. S13c in Supporting information). Moreover, the absorption of **B-C-Pt** NPs is stable within a week (Fig. S13d in Supporting information). These results indicated that **B-C-Pt** NPs have well long-term stability in water. The encapsulation yield of **B-C-Pt** in NPs was calculated be 93.3% [48].

Due to its red-shifted absorption peak, the $^1O_2$ generation ability of **B-C-Pt** NPs was investigated under 808 nm laser irradiation using singlet oxygen sensor green (SOSG) as a $^1O_2$ probe. The fluorescence of SOSG in presence of **B-C-Pt** NPs increased with irradiation time (Fig. 2f), but slightly changed in the absence of **B-C-Pt** NPs (Fig. S14a in Supporting information). Using ICG as a reference ($^1O_2$ quantum yield = 0.8%), the $^1O_2$ quantum yield of **B-C-Pt** NPs was calculated to be 4.0% (Fig. S14b in Supporting information). Next, the photothermal conversion performance of **B-C-Pt** NPs was studied. The temperature of **B-C-Pt** NPs solution varied with laser power and concentration. Upon irradiation with 808 nm laser (0.75 W/cm$^2$) for 10 min, the temperature of 15 μmol/L **B-C-Pt** NPs solution rapidly increased to 57.5 °C (Fig. S15 in Supporting information), which can effectively kill cancer cells. According to Fig. 2g, the PCE of **B-C-Pt** NPs was 40.6% ± 0.8% ($n$ = 3). Owing to its strong NIR absorbance and good PCE, **B-C-Pt** NPs exhibited excellent PA imaging capability. As illustrated in Fig. 2h, a positive relationship between PA signal intensity and **B-C-Pt** NPs concentration was obtained.

Green fluorescence of reaction product between 2,7-dichlorodihydrofluorescein diacetate (DCFH-DA) and $^1O_2$ was observed in cells in the **B-C-Pt** NPs + Laser group (Fig. 3a), but was not observed in cells in phosphate buffer salt solution (PBS), PBS + Laser, and **B-C-Pt** NPs groups, suggesting intracellular $^1O_2$ generation of **B-C-Pt** NPs. Previous reports confirmed that a pyridine-platinum complex could target mitochondria. We used JC-1 assay to evaluate the mitochondria-targeting capability of **B-C-Pt** NPs, as its NIR fluorescence exceeds the detection range of a confocal fluorescent microscope. Compared with that of cells in the PBS + Laser and **B-C-Pt** NPs groups, the intensity of red fluorescence of cells in the **B-C-Pt** NPs + Laser group obviously decreased, and the intensity of their green fluorescence significantly increased (Fig. S16 in Supporting information). This observation indicates that **B-C-Pt**

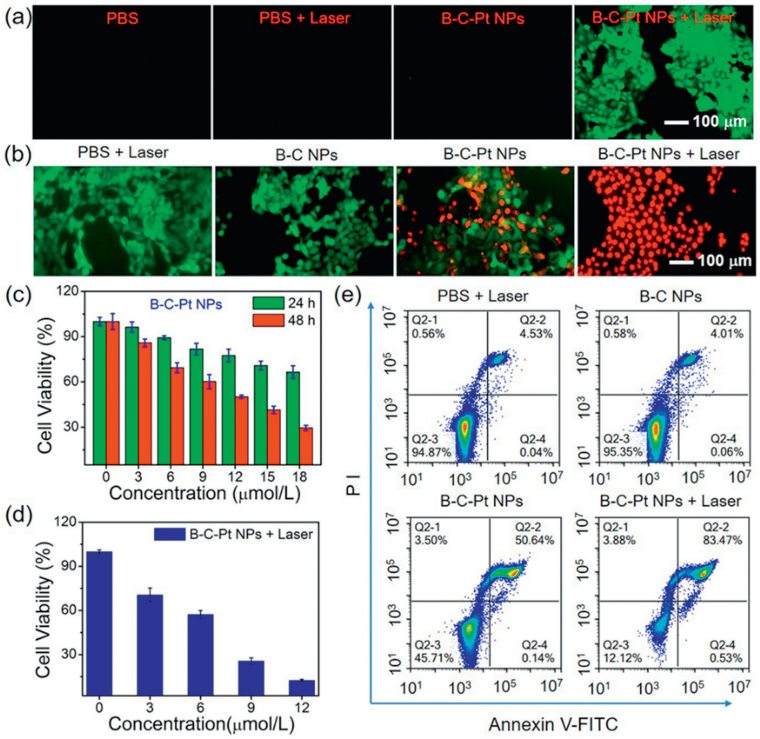


**Fig. 3.** Fluorescent images of 4T1 cells in different treatment groups: (a) cells were incubated with DCFH-DA and (b) co-stained with calcein AM and PI (Scale bar: 100 μm). (c) Viability of 4T1 cells incubated with **B-C-Pt** NPs for 24 and 48 h and (d) **B-C-Pt** NPs + Laser. (e) Flow cytometric analysis of the death of cells in different groups.

NPs could possibly target mitochondria, and $^1O_2$ generated upon laser irradiation could destroy the mitochondrial membrane and decrease its potential.

Calcein AM (green fluorescence) and propidium iodide (PI) (red fluorescence) were applied to visualize the cell damage. Cells in the PBS + Laser and **B-C** NPs groups only exhibited green fluorescence, while those in the **B-C-Pt** NPs group exhibited both green and red fluorescence (Fig. 3b), an indication that part of cells were dead by chemotherapy. Further, cells in the **B-C-Pt** NPs + Laser group only exhibited red fluorescence, indicative of excellent therapeutic efficacy of the combined chemotherapy and phototherapy.

Methyl thiazolyl tetrazolium (MTT) assay can quantitatively evaluate the dark toxicity and phototoxicity of **B-C-Pt** NPs. Upon incubating with 18 μmol/L **B-C-Pt** NPs for 24 and 48 h in darkness, the viability of 4T1 cells gradually decreased to 66.4% and 29.5%, respectively (Fig. 3c). The 50% inhibitory concentration ($IC_{50}$) of **B-C-Pt** NPs in darkness (48 h) was determined to be 12.3 μmol/L. In contrast, the dark toxicity of **B-C** NPs was negligible (Fig. S17 in Supporting information). This indicates that cisplatin remained cytotoxic after being chelated with **B-C**. After incubating with 12 μmol/L **B-C-Pt** NPs, 4T1 cells were exposed to laser irradiation. The cell viability significantly decreased to 12.5% (Fig. 3d), and the $IC_{50}$ value of **B-C-Pt** NPs + Laser is 6.8 μmol/L. The cell viability of 4T1 cells treated with 20 μmol/L **B-C** NPs + Laser was decreased to 26.6%. The $IC_{50}$ value of **B-C** NPs + Laser is 13.6 μmol/L (Fig. S17). These results demonstrated that **B-C-Pt** NPs are effective in synchronous PDT, PTT, and chemotherapy.

Flow cytometry experiments were conducted to further confirm the death pathways of cells. Live cells cannot be stained with Annexin V-fluorescein isothiocyanate (FITC) and PI because their cell membrane is complete and normal, and located in Q2-3 area. In early apoptosis, phosphatidylserine turns from the inner surface of the cell membrane to the outer surface of the cell membrane but the cell membrane is complete, thus the early apoptotic cells can only be stained with Annexin V-FITC, and located in Q2-4 area. The cell membrane of late apoptotic and necrotic cells is broken, cells membrane and DNA were stained with Annexin V-FITC and PI, respectively, and located in Q2-2 area. Compared with that of cells in the PBS + Laser and **B-C** NPs group, the late apoptotic/necrotic rate of cells in the **B-C-Pt** NPs and **B-C-Pt** NPs + Laser group increased to 50.6% and 83.5%, respectively (Fig. 3e). This result indicates the death of cells treated with **B-C-Pt** NPs + Laser is mainly *via* late apoptosis and necrosis.

All the animal experiments were approved by the Ethics Committee for Experimental Animal Welfare of Hunan Normal University. The strong NIR II fluorescent and PA signals in the tumor of mice intratumorally injected with **B-C-Pt** NPs demonstrated its excellent *in vivo* fluorescent and PA imaging ability (Figs. 4a and b). *In vivo* heat generation capability of **B-C-Pt** NPs was determined by infrared thermal images of mice. Upon laser irradiation for 2 min, the temperature of tumor injected with **B-C-Pt** NPs rapidly increased from 30.2 °C to 53.3 °C and then slowly increased to 57.6 °C in the following 8 min (Fig. 4d). However, the temperature of tumor treated with PBS + Laser only increased from 31.5 °C to 35.3 °C (Fig. 4c).

*In vivo* antitumor capability of **B-C-Pt** NPs was investigated. Twenty 4T1 tumor-bearing BALB/c mice were divided into four groups ($n$ = 5 for each group) as follows: PBS, PBS + Laser, **B-C-Pt** NPs, and **B-C-Pt** NPs + Laser. As shown in Fig. 4e, the tumor volume of mice in the PBS and PBS + Laser groups increased by ~10 fold, but **B-C-Pt** NPs can partially inhibit the growth of tumors. Further, the tumor was completely inhibited by **B-C-Pt** NPs + Laser. Moreover, the weight of mice was almost unchanged during the monitoring period (Fig. 4f). Next, main organs (heart, liver, spleen, lung, and kidney) and tumor tissues of mice that underwent **B-C-Pt** NPs + Laser treatment were collected. The hematoxylin and eosin (H&E) staining results (Fig. 4g and Fig. S18 in Supporting information) demonstrated that the tumor tissue was damaged, while organs remained healthy. The Ki-67 stain-

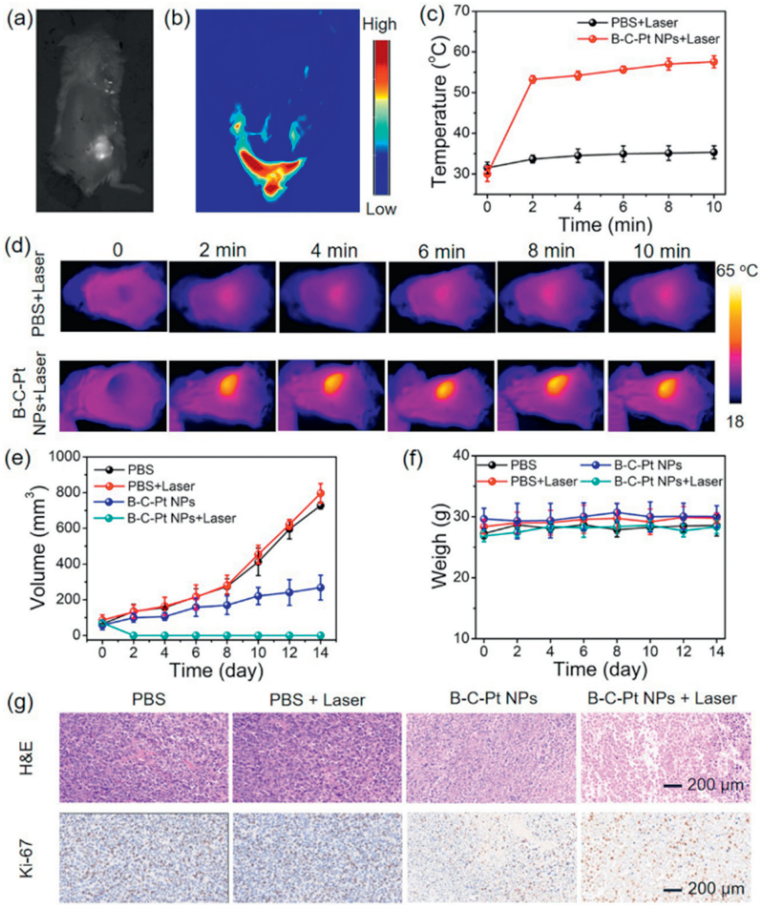


**Fig. 4.** (a) *In vivo* NIR II FL and (b) PA imaging of **B-C-Pt** NPs in tumor-bearing mice. (c) The temperature change and (d) corresponding infrared thermographic images of tumor tissue of mice intratumorally injected with PBS or **B-C-Pt** NPs, followed by 808 nm laser irradiation. Change of (e) tumor volume and (f) weight of mice in different treatment groups. (g) Images of H&E- and Ki-67-stained tumor tissues of mice in different treatment groups (Scale bar: 200 μm).

ing further revealed that the tumor cell proliferation was effectively inhibited. All the above results confirmed that **B-C-Pt** NPs are promising photo-chemotheranostic agents.

In conclusion, we developed three D-$\pi$-A-structured BODIPY derivatives with high absorption coefficients and strong fluorescence in NIR region. The absorption and fluorescence spectra of BODIPY were red-shifted due to the enlarged $\pi$-conjugated structures and the strong ICT effect induced by cisplatin modification. The heavy atom effect of Pt could obviously improve the $^1O_2$ generation capability of **B-C-Pt**. Based on that, **B-C-Pt** NPs were encapsulated by DSPE-PEG-2000. The H-type aggregation of **B-C-Pt** in water was inhibited, red-shifting the absorption and fluorescence emission of **B-C-Pt** NPs to 762 and 985 nm, respectively. The $^1O_2$ generation quantum yield and PCE of **B-C-Pt** NPs were measured to be 4.0% and 40.6%, respectively. Exposed to 808 nm laser, **B-C-Pt** NPs still generated $^1O_2$ in cells, damaging mitochondrion to facilitate tumor cell death. In addition, **B-C-Pt** NPs the presence of cisplatin enabled **B-C-Pt** to have good chemotherapeutic effect, the $IC_{50}$ value of **B-C-Pt** NPs is 12.3 μmol/L. The viability of 4T1 cells treated with 12 μmol/L **B-C-Pt** NPs + Laser was decreased to 12.5%. **B-C-Pt** NPs displayed well *in vivo* fluorescence and PA imaging ability, and removed tumor tissue under laser irradiation. Finally, *in vitro* and *in vivo* studies confirmed that **B-C-Pt** NPs are promising multifunctional photo-chemotheranostic agents for NIR II fluorescent and PA imaging-guided combined phototherapy and chemotherapy for cancer treatment. This work provided an important example for the development of multifunctional photo-chemotheranostic agents.

## Declaration of competing interest

The authors declare that they have no known competing financial interests or personal relationships that could have appeared to influence the work reported in this paper.

## Acknowledgments

This work was supported by National Natural Science Foundation of China (No. 62175262), the Science and Technology Innovation Program of Hunan Province (No. 2022RC1201), the Fundamental Research Funds for the Central Universities of Central South University (No. 2019zzts849).

## Supplementary materials

Supplementary material associated with this article can be found, in the online version, at doi:10.1016/j.cclet.2023.108467.

## References

[1] D. Xi, N. Xu, X. Xia, et al., Adv. Mater. 34 (2022) 2106797.
[2] K. Yang, B. Yu, M. Lan, et al., Chin. Chem. Lett. 34 (2023) 107889.
[3] J. Zhao, Y. Yang, X. Xu, et al., Angew. Chem. Int. Ed. 61 (2022) 202210920.
[4] X. Yang, T. Yang, Q. Liu, et al., Adv. Funct. Mater. 32 (2022) 2206346.
[5] X. Li, F. Fang, B. Sun, et al., Nanoscale Horiz. 6 (2021) 177–185.
[6] J.N. Liu, W. Bu, J. Shi, Chem. Rev. 117 (2017) 6160–6224.
[7] Q. Cheng, Z.H. Li, Y.X. Xia, et al., NPG Asia Mater. 11 (2019) 63.
[8] R. Lima-Sousa, B.L. Melo, C.G. Alves, et al., Adv. Funct. Mater. 31 (2021) 2010777.

[9] F. Yang, Z. Zhao, B. Sun, et al., Trends Cancer 6 (2020) 645–659.
[10] Y. Liu, M. Zhu, M. Meng, et al., Chin. Chem. Lett. 34 (2022) 107583.
[11] Z. Tu, I.S. Donskyi, H. Qiao, et al., Adv. Funct. Mater. 30 (2020) 200093.
[12] M. Chen, N. Gong, W. Sun, et al., Small 18 (2022) 2201672.
[13] J. Liu, C. Zhu, L. Xu, et al., Nano Lett. 20 (2020) 8102–8111.
[14] Y. Yang, Y. Zhang, R. Wang, et al., Chin. Chem. Lett. 33 (2022) 4583–4586.
[15] Z. Xie, T. Fan, J. An, et al., Chem. Soc. Rev. 49 (2020) 8065–8087.
[16] L. Wu, X. Cai, H. Zhu, et al., Adv. Funct. Mater. 28 (2018) 1804324.
[17] L. Xu, J. Liu, J. Xi, et al., Small 14 (2018) 1800785.
[18] M. Li, X. Sun, N. Zhang, et al., Adv. Sci. 5 (2018) 1800155.
[19] C. Yan, Y. Zhang, Z. Guo, Coord. Chem. Rev. 427 (2021) 213556.
[20] L. Liu, W. Qiu, B. Liu, et al., Adv. Funct. Mater. 26 (2016) 6257–6269.
[21] J. Xu, W. Han, P. Yang, et al., Adv. Funct. Mater. 28 (2018) 1803804.
[22] H. Meng, L. Lu, X. Zhao, et al., Anal. Chem. 87 (2015) 4448–4454.
[23] Q. Wu, G. Chen, K. Gong, et al., Matter 1 (2019) 496–512.
[24] W. Liu, Y. Wang, Y. Li, et al., Small 13 (2017) 1603459.
[25] Y. Wang, G. Wei, X. Zhang, et al., Adv. Mater. 29 (2017) 1605357.
[26] X. Ma, T. Zhang, W. Qiu, et al., Chem. Eng. J. 420 (2021) 127657.
[27] J. Tian, C. Yao, W. Yang, et al., Chin. Chem. Lett. 28 (2017) 798–806.
[28] B. Chen, L. Mei, R. Han, et al., Chin. Chem. Lett. 32 (2021) 1775–1779.
[29] B. Ding, P. Zheng, P. Ma, et al., Adv. Mater. 32 (2020) 1905823.
[30] W. Fan, B. Yung, P. Huang, et al., Chem. Rev. 117 (2017) 13566–13638.
[31] Z. Ye, M. Ji, K. Wu, et al., Angew. Chem. Int. Ed. 61 (2022) e202204518.
[32] M. Su, Q. Han, X. Yan, et al., ACS Nano 15 (2021) 5032–5042.
[33] V.N. Nguyen, Y. Yim, S. Kim, et al., Angew. Chem. Int. Ed. 59 (2020) 8957–8962.
[34] X. Xue, C. Qian, H. Fang, et al., Angew. Chem. Int. Ed. 58 (2019) 12661–12666.
[35] B. Liu, J. Jiao, W. Xu, et al., Adv. Mater. 33 (2021) 2100795.
[36] Y. Qin, X. Liu, P. Jia, et al., Chem. Soc. Rev. 49 (2020) 5678–5703.
[37] G. Li, X. Zhang, W. Zhao, et al., ACS Appl. Mater. Interfaces 12 (2020) 20180–20190.
[38] V. Ramu, P. Kundu, P. Kondaiah, et al., Inorg. Chem. 60 (2021) 6410–6420.
[39] J. Zhou, Y. Zhang, G. Yu, et al., J. Am. Chem. Soc. 140 (2018) 7730–7736.
[40] V. Ramu, S. Gautam, A. Garai, et al., Inorg. Chem. 57 (2018) 1717–1726.
[41] Z. Guo, Y. Zou, H. He, et al., Adv. Mater. 28 (2016) 10155–10164.
[42] X. Lv, T. Han, Y. Wu, et al., Chem. Commun. 57 (2021) 9744–9747.
[43] R. Padrutt, V. Babu, S. Klingler, et al., ChemMedChem 16 (2021) 694–701.
[44] Z. Zhao, C. Chen, W. Wu, et al., Nat. Commun. 10 (2019) 768.
[45] X. Xing, K. Yang, B. Li, et al., J. Phys. Chem. Lett. 13 (2022) 7939–7946.
[46] E. Feng, Y. Liu, S. Lv, et al., Adv. Funct. Mater. 28 (2022) 2209258.
[47] D. Xi, M. Xiao, J. Cao, et al., Adv. Mater. 32 (2020) 1907855.
[48] D. Zhu, W. Xie, Y. Xiao, et al., Nanotechnology 29 (2018) 084002.